

Planned seismic imaging using explicit one-way operators

Robert J. Ferguson¹ and Gary F. Margrave²

ABSTRACT

A method is presented to compare the accuracy and computational cost of explicit one-way extrapolation operators as used in seismic imaging. For a given model, accuracy is measured in terms of lateral positioning error, and cost is calculated relative to the cost of the spatial fast Fourier transform. The result is a planned imaging scheme that achieves the greatest accuracy with respect to the velocity model for a fixed cost.

To demonstrate, we use a 2D section of the EAGE/SEG salt model and assemble a suite of the most common operators. The data are imaged using each operator individually, and the results are compared to the result from the plan-based algorithm. The planned image is shown to return improved accuracy for no additional cost.

INTRODUCTION

The one-way extrapolation operators that are central to the recursive-extrapolation approach to seismic imaging arise from approximate solutions to the wave equation. They are constructed with respect to depth z such that reflections caused by the component of the velocity gradient in the z direction are suppressed. The solution is approximate in that the lateral variation in elastic parameters is assumed to be weak such that the propagating wavefield does not generate other scattered wavefields.

Since the first one-way extrapolators were implemented using computers, numerous operators have been developed. Basic operators, like implicit finite difference (Claerbout, 1971), explicit finite difference (Berkhout, 1979), phase shift (Gazdag, 1978), and split-step Fourier (Stoffa et al., 1990), have been improved over the years, resulting in a large number of possibilities for use in seismic imaging.

The decision to use one operator over another is often based entirely on qualitative comparisons (see, for example, Thorbecke and Berkhout, 1994; Han, 1998) made for a specific geographic region. For example, imaging methods based on explicit finite difference may be favored in areas with significant lateral variation and not much dip. In areas of high dip, methods related to phase shift plus interpolation (Gazdag and Sguazzero, 1984) or split-step Fourier (Stoffa et al., 1990) may be preferred.

In general, a region may have lateral complexity that changes with depth, so that imaging is not necessarily optimal in both cost and performance. The accuracy of any explicit operator can be increased, of course, but this usually results in increased computational cost. Instead, a set of similar-cost operators should be available, and the operator best suited to the complexity of each level in the model selected “on the fly” during imaging. Selection, of course, requires quantification of both accuracy and computational cost.

Quantitative analysis of operators is usually done to compute a correction to a given operator for a given medium [for example, Nautiyal et al. (1993)]. Such approaches result in improved operators, but do little to illuminate important differences between operators.

To quantify the relative performance of different operators, a unifying description is required, and we find such a description in the Fourier integral operator. Fourier integral operators are well known in the mathematical literature (see, for example, Hörmander, 1965; Kumano-Gō, 1981; Duistermaat, 1995), and geophysicists have recently recognized their importance as extrapolation operators of seismic waves. Early mention is given by Black et al. (1984), who postulate that a similar mathematical form allows seismic waves to be extrapolated through complicated media without loss of accuracy. Fishman and McCoy (1985) provide an extensive mathematical description in the context of extrapolating acoustic waves in water.

More recently, Margrave and Ferguson (1997) recognize that the commonly implemented phase-shift-plus-interpolation method of Gazdag and Sguazzero (1984) approaches

Manuscript received by the Editor April 23, 2003; revised manuscript received February 24, 2005; published online September 14, 2005.

¹University of Texas at Austin, Department of Geological Sciences, Campus Mail Code C1100, Austin, Texas 78712-0254. E-mail: fergusonr@mail.utexas.edu.

²University of Calgary, Department of Geology and Geophysics, 2500 University Drive NW, Calgary, Alberta T2N 1N4, Canada. E-mail: gary@crewes.org.

© 2005 Society of Exploration Geophysicists. All rights reserved.

a Fourier integral operator when implemented for continuous model variation. Similarly, Le Rousseau and de Hoop (2001) recognize that the commonly implemented phase-screen method of We and Huang (1992) asymptotically approaches a Fourier integral operator as the accuracy of that operator is increased.

We use the Fourier integral operator as a basis for comparison between the approximations that underlie the different operators. Analogous to the Li correction (Li, 1991), we compute the phase error associated with each operator for a given velocity variation. Then, to provide physical meaning, we relate this error to the error in the lateral position that results from extrapolation. We find that, because positioning error increases monotonically with wavenumber, the error needs to be computed only for a maximum phase angle of interest to facilitate meaningful comparison between operators.

This approach is found to have negligible added cost compared to the cost of extrapolation, and we use it to create operator “plans” for seismic imaging. That is, for each depth level, one of the available one-way operators is assigned by selecting the one with the lowest error for a fixed cost. Alternatively, plans can be devised that assign operators based on minimum cost for a fixed error.

We examine a few of the more common one-way operators to gain insight into the relationships between accuracy and computational cost. Of course, owing to the wide range of choices, our set of one-way operators is not intended to represent the ideal set, and in no way do they represent optimal implementations. In practice, others may find that error and cost estimates differ somewhat from those used here.

THEORY

The scalar wave equation for monochromatic-seismic wavefields can be written

$$\nabla^2 \psi(\mathbf{x}, z) = [ik(\mathbf{x}, z)]^2 \psi(\mathbf{x}, z), \quad (1)$$

where z and $\mathbf{x} = (x_1, x_2)$ are the coordinates of depth (z) and the two lateral dimensions (x_1, x_2), respectively. Operator ∇^2 is the spatial Laplacian, and

$$k(\mathbf{x}, z, \omega) = \frac{\omega}{v(\mathbf{x}, z)}, \quad (2)$$

is a spatially varying wavenumber associated with temporal frequency ω .

Assuming $\partial_z v(\mathbf{x}, z) = 0$ for $z_0 \leq z \leq z_0 + \Delta z$, where z_0 is a reference depth and $\partial_x v(\mathbf{x}, z)$ is small [thin-slab approximation; see, for example, Berkhout (1985, 327) and Wu and de Hoop (1996)], a pseudodifferential operator [Saint Raymond (1991, chapter 2) provides a good definition] is found for the j th derivative of ψ along z (Margrave and Ferguson, 2000):

$$\partial_z^j \psi \approx \frac{1}{(2\pi)^2} \int_{-\infty}^{\infty} [ik_z(\mathbf{x}, \mathbf{k}_x)]^j \varphi(\mathbf{k}_x) e^{-i\mathbf{k}_x \cdot \mathbf{x}} d\mathbf{k}_x, \quad (3)$$

where $\mathbf{k}_x = (k_{x1}, k_{x2})$ are the spatial wavenumbers corresponding to \mathbf{x} , and

$$\varphi(\mathbf{k}_x) = \int_{-\infty}^{\infty} \psi(\mathbf{x}) e^{i\mathbf{k}_x \cdot \mathbf{x}} d\mathbf{x}. \quad (4)$$

The Taylor series expansion of the desired wavefield $\psi(z + \Delta z)$ about a known wavefield $\psi(z)$ is (Berkhout, 1985, 324)

$$\psi(\mathbf{x}, z + \Delta z) = \psi(\mathbf{x}, z) + \sum_{j=1}^{\infty} \frac{1}{(j-1)!} [\partial_z^j \psi(\mathbf{x}, z)] \Delta z^j, \quad (5)$$

where Δz is positive or negative depending on the desired direction of propagation. Upon replacement of ∂_z^j with equation 3, and summing the resulting infinite series to a complex exponential (Margrave and Ferguson, 2000), a Fourier integral operator equation for one-way extrapolation results:

$$\begin{aligned} \psi(\mathbf{x}, z + \Delta z) \\ = \frac{1}{(2\pi)^2} \int_{-\infty}^{\infty} \varphi(\mathbf{k}_x, z) \alpha(\mathbf{x}, \mathbf{k}_x, \Delta z) e^{i\mathbf{k}_x \cdot \mathbf{x}} d\mathbf{k}_x, \end{aligned} \quad (6)$$

where extrapolation symbol α is given by

$$\alpha(\mathbf{x}, \mathbf{k}_x, \Delta z) = e^{i\Delta z k_z(\mathbf{x}, \mathbf{k}_x)}. \quad (7)$$

In practice, suppression of evanescent energy is required (Berkhout, 1985, 286), so wavenumbers k_z are computed:

$$\begin{aligned} k_z(\mathbf{x}, \mathbf{k}_x) \\ = \begin{cases} \operatorname{sgn}(\Delta z) k(\mathbf{x}) \sqrt{1 - \frac{|\mathbf{k}_x|^2}{k^2(\mathbf{x})}} & \text{if } \frac{|\mathbf{k}_x|^2}{k^2(\mathbf{x})} \leq 1 \\ i \operatorname{sgn}(\Delta z) k(\mathbf{x}) \sqrt{1 - \frac{|\mathbf{k}_x|^2}{k^2(\mathbf{x})}} & \text{if } \frac{|\mathbf{k}_x|^2}{k^2(\mathbf{x})} > 1 \end{cases}, \end{aligned} \quad (8)$$

where $\operatorname{sgn}()$ is the signum function.

Use of equation 6 for wavefield extrapolation is costly (Holberg, 1988; Pai, 1988). For each Δz and ω , extrapolation is computed as a $\mathbf{k}_x \rightarrow \mathbf{x}$ transform where the spatial variation of α precludes use of the fast Fourier transform (FFT) (Black et al., 1984; Holberg, 1988). Computational cost is controlled by the number of traces in the inline N and crossline M directions, the number of frequencies ω , and the number of depths through which extrapolation is to be applied. For example, extrapolation of a single ω through Δz has a cost $\propto N^2 M^2$.

Most operators used in seismic imaging achieve computational efficiency by approximating α as a series of separable terms such that

$$\alpha(\mathbf{x}, \mathbf{k}_x) \approx \sum_{j=0}^n a_j(\mathbf{x}) b_j(\mathbf{k}_x), \quad (9)$$

where n is the number of terms in the series. Extrapolation is then approximated by

$$\begin{aligned} \psi(\mathbf{x}, z + \Delta z) \\ \approx \sum_{j=0}^n a_j(\mathbf{x}) \frac{1}{(2\pi)^2} \int_{-\infty}^{\infty} \varphi(\mathbf{k}_x, 0) b_j(\mathbf{k}_x) e^{i\mathbf{k}_x \cdot \mathbf{x}} d\mathbf{k}_x. \end{aligned} \quad (10)$$

Using this series representation for $\psi(z + \Delta z)$, computational cost is proportional to the number of terms n in the series times the cost of the FFT, or $nMN \log MN$ — a significant savings over the Fourier integral operator.

Selection of operators

Examining the most basic ω - x operator (Berkhout, 1985, 338) shows that coefficients a_j are given by

$$a_{j,\omega-x} = e^{i\Delta z k(\mathbf{x})} \gamma_j(\mathbf{x}), \quad (11)$$

where γ_j for $j = [0, 1, 2, 3, 4]$ are given in Table 1, and

$$b_{j,\omega-x} = |\mathbf{k}_x|^{2j}. \quad (12)$$

In practice, b_j are implemented in the \mathbf{x} domain using finite differences, though cost savings can be small when high-fidelity difference operators are implemented (Holberg, 1988).

The generalized screen (GS) operator (Le Rousseau and de Hoop, 2001) is analyzed in a similar way. For the GS operator, coefficients $a_{j,GS}$ are written

$$a_{j,GS} = e^{i\Delta z [k(\mathbf{x}) - \bar{k}]} \lambda_j(\mathbf{x}), \quad (13)$$

where $\bar{k} = \text{MAX}[k(\mathbf{x})]$, with λ_j given in Table 2. The corresponding $b_{j,GS}$ are given by

$$b_{j,GS} = e^{i\Delta z \bar{k}_z(\mathbf{k}_x)} \kappa_j(\mathbf{k}_x), \quad (14)$$

where $\bar{k}_z(\mathbf{k}_x) = \bar{k} \sqrt{1 - |\mathbf{k}_x|^2 / \bar{k}^2}$, with κ_j given in Table 2. In practice, because α_{GS} is nonunitary, a normalization procedure is used to stabilize the GS operator (Le Rousseau and de Hoop, 2001).

The ω - x and GS operators are derived by expanding the square root and exponential terms in α , and many other operators exist in this class (for example, Hale, 1991; Ristow and Ruhl, 1994; Wu et al., 1997), and each is amenable for analysis using equations 9 and 10.

The ω - x operator, again for example, is very accurate within a limited range of \mathbf{k}_x and tolerates strong velocity variation (Berkhout, 1985). Figure 1 shows that, even for constant velocity, the ω - x approximation is accurate only for a limited range of \mathbf{k}_x . This is usually referred to as the dip-limited nature of these operators and is the result of the nonunitary nature of

Table 1. ω - x variables.

j	γ_j
0	1
1	$-\frac{i\Delta z}{2k}$
2	$\frac{-1/8i\Delta z k - 1/8\Delta z^2 k^2}{k^4}$
3	$\frac{-1/16i\Delta z k - 1/16\Delta z^2 k^2 + 1/48i\Delta z^3 k^3}{k^6}$
4	$\frac{-5/128i\Delta z k - 5/128\Delta z^2 k^2 + 1/64i\Delta z^3 k^3 + 1/384\Delta z^4 k^4}{k^8}$

Table 2. GS variables.

j	0	1	2	3	4
λ_j	1	$-\frac{i\Delta z}{2}(\bar{k}^2 - k^2)$	$\frac{i\Delta z}{8}(\bar{k}^2 - k^2)^2$	$-\frac{i\Delta z}{16}(\bar{k}^2 - k^2)^3$	$\frac{5i\Delta z}{128}(\bar{k}^2 - k^2)^4$
κ_j	1	$\bar{k}_z^{-1} - \bar{k}^{-1}$	$\bar{k}_z^{-3} - \bar{k}^{-3}$	$\bar{k}_z^{-5} - \bar{k}^{-5}$	$\bar{k}_z^{-7} - \bar{k}^{-7}$

the operator beyond $|\mathbf{k}_x| = 0$. For smaller values of \mathbf{k}_x , the ω - x approximation is very good even in laterally varying media, as shown in Figure 2. (In Figures 1 and 2, $k_{z,\omega-x}$ is computed as the phase of $\alpha_{\omega-x}$ for $\Delta z = 1$.)

The GS operator is accurate for a greater range of \mathbf{k}_x but can be restricted to weaker lateral velocity variation than is the ω - x operator. This is because of the branch point at $\bar{k}_z = 0$ (Le Rousseau and de Hoop, 2001) and the requirement that $\bar{k} = \text{MAX}[k(\mathbf{x})]$. For constant velocity $k = \bar{k}$, the GS approximation is accurate up to the evanescent boundary $|\mathbf{k}_x| = k$, as is shown in Figure 1. For variable velocity (for example, in Figure 2), the approximation becomes less accurate with increasing velocity. (In Figures 1 and 2, $k_{z,GS}$ is computed as the phase of α_{GS} for $\Delta z = 1$.)

The phase-shift-plus-interpolation (PSPI) operator of Gazdag and Sguazzero (1984) represents a different approach to the factorization of α . Instead of factorizing α directly, velocity variation is approximated using a set of j reference velocities so that (Margrave and Ferguson, 1997)

$$a_{j,PSPI}(\mathbf{x}) = e^{i\Delta z [k(\mathbf{x}) - \bar{k}_j]} \Omega_j(\mathbf{x}), \quad (15)$$

where $\bar{k}_j = \omega/v_j$ is the vertical wavenumber corresponding to reference velocity v_j for normal incidence, and

$$\Omega_j(\mathbf{x}) = \begin{cases} 1 & \text{if } v(\mathbf{x}) = v_j \\ 0 & \text{if } v(\mathbf{x}) \neq v_j. \end{cases} \quad (16)$$

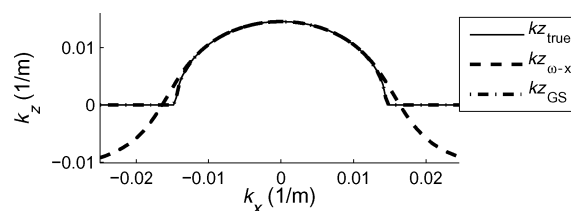


Figure 1. Constant velocity and frequency ($k = \omega/v$) is used to compute k_z associated with the ω - x operator. The departure of the $k_{z,\omega-x}$ curve (dashed) from the true curve (solid) is due, in this example, to truncating α at $n = 4$ (equation 9). Error increases with k_x . For comparison, $k_{z,GS}$ is plotted for this model (dotted), and it is clearly a better approximation as it is identical with the true curve.

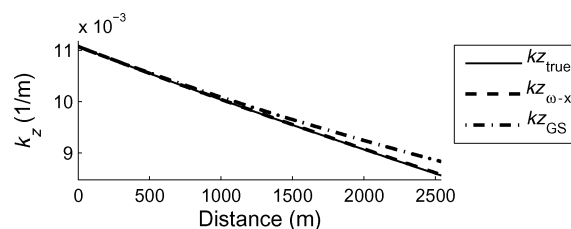


Figure 2. Vertical wavenumber for a linear-varying velocity (increasing from left to right) associated with the GS operator. Error can be seen in the departure of $k_{z,GS}$ (dashed) from the true curve (solid) for increasing velocity. This error is the result, here, of truncating α at $n = 4$ (equation 9). For comparison, $k_{z,\omega-x}$ is plotted for this model (dotted), and is clearly a better approximation (for the given ω and $v(x)$, the $k_{z,\omega-x}$ is nearly exact for the value of k_x).

Coefficients b_j for the PSPI operator are

$$b_{j,\text{PSPI}}(\mathbf{k}_x) = e^{i\Delta z[\bar{k}_{z,j}(\mathbf{k}_x)]}, \quad (17)$$

where $\bar{k}_{z,j}(\mathbf{k}_x) = \bar{k} \sqrt{1 - |\mathbf{k}_x|^2 / \bar{k}_j^2}$.

Coefficients $a_{j,\text{PSPI}}$ actually represent the correction and the windowing operations in the extended split-step operator (Kessinger, 1992). For PSPI as described by Gazdag and Sguazzero (1984), $a_{j,\text{PSPI}} = \Omega_j$, and a smooth summation of the j extrapolated wavefields is accomplished by tapering $\Omega_j(\mathbf{x})$. For selection of v_j and Ω_j , Bagaini et al. (1995) use a statistical approach that returns very good results.

PSPI tolerates strong lateral contrasts in velocity at large phase angles (for example, the transition from homogeneous sediment to salt, as in Figure 3). Here, two reference velocities ($n=2$ in equation 10) are sufficient for maximum accuracy. When variation is smooth (as in Figure 4), however, many more reference velocities are required, and cost may increase dramatically.

Other operators that factor α based on velocity variation (as opposed to series expansion) can be analyzed using equations 9 and 10. Examples are the generalized f - k operator of Pai (1988), the generalized phase-shift operator of Kosloff and Kessler (1987), and the variable-length-transform method of Benson (1995). Though these operators are all implemented as efficient, band-limited convolutions in the wavenumber domain, they effectively gain efficiency by low-pass filtering the velocity variation. We refer to these operators as the band-limited (BL) class.

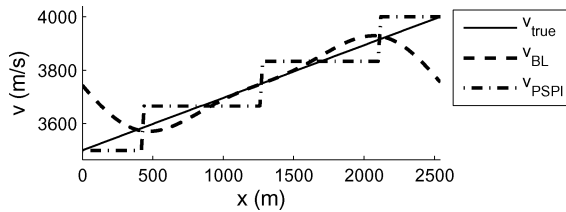


Figure 3. Linear variation in velocity (solid) and the corresponding PSPI approximation (dashed). The error in imaging using PSPI is due to departure from the true velocity. The velocity approximation for an equivalent (similar cost) band-limited (BL) operator is plotted (dotted). Assuming that zero padding is associated with $x < 500$ m and $x > 2500$ m, the BL approximation is closer to the model than the PSPI approximation.

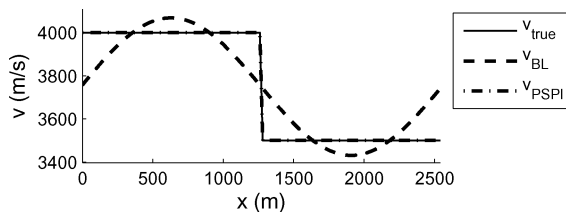


Figure 4. Step variation in velocity (solid) and the corresponding BL approximation (dashed). Error in imaging using BL is due to departure from the true velocity. The velocity approximation corresponding to an equivalent (similar cost) PSPI operator is plotted (dotted) for comparison. For this model, the PSPI approximation is much closer (identical) to the true model.

BL operators are based on the observation that, in equation 6, product $\varphi(z)\alpha(\Delta z)$ can be computed as a convolution in the full Fourier domain (Margrave and Ferguson, 1997). To see this, compute the Fourier transform of equation 6:

$$\varphi(\mathbf{k}'_x, z + \Delta z) = \int_{-\infty}^{\infty} \varphi(\mathbf{k}_x, z) A(\mathbf{k}'_x - \mathbf{k}_x, \mathbf{k}_x, \Delta z) d\mathbf{k}_x, \quad (18)$$

where

$$A(\mathbf{k}'_x - \mathbf{k}_x, \mathbf{k}_x, \Delta z) = \int_{-\infty}^{\infty} \alpha(\mathbf{x}, \mathbf{k}_x, \Delta z) e^{-i\mathbf{x} \cdot [\mathbf{k}'_x - \mathbf{k}_x]} d\mathbf{x}. \quad (19)$$

As a discrete convolution, equation 18 is calculated (Appendix A):

$$\begin{aligned} \varphi_{j,k}(z + \Delta z) &= \frac{1}{M} \sum_{p=-M/2}^{M/2-1} \frac{1}{N} \sum_{q=-N/2}^{N/2-1} \varphi(z)_{j-p;k-q} A(\Delta z)_{p,j-p;q,k-q}, \end{aligned} \quad (20)$$

where indices $\{-M/2 \leq j \leq M/2-1\}$ and $\{-N/2 \leq k \leq N/2-1\}$ correspond to wavenumbers $k_{x1,j} = j\Delta k_{x1}$ and $k_{x2,k} = k\Delta k_{x2}$. Extrapolated wavefield $\psi(z + \Delta z)$ is the inverse Fourier transform of equation 20:

$$\psi(\mathbf{x}, z + \Delta z) = \frac{1}{(2\pi)^2} \int_{-\infty}^{\infty} \varphi(\mathbf{k}_x, z + \Delta z) e^{-i\mathbf{k}_x \cdot \mathbf{x}} d\mathbf{k}_x. \quad (21)$$

For efficiency, replace M and N in equation 20 with $m \ll M$ and $n \ll N$, so that spectrum

$$\begin{aligned} \tilde{\varphi}_{j,k}(z + \Delta z) &= \frac{1}{M} \sum_{p=-m/2}^{m/2-1} \frac{1}{N} \sum_{q=-n/2}^{n/2-1} \varphi(z)_{j-p;k-q} A(\Delta z)_{p,j-p;q,k-q}, \end{aligned} \quad (22)$$

is now an approximation $\tilde{\varphi}(z + \Delta z) \approx \varphi(z + \Delta z)$ to the true spectrum. For $\Delta k_{x,1} = 1/\Delta x_1 M$ and $\Delta k_{x,2} = 1/\Delta x_2 N$, where $\Delta \mathbf{x} = (\Delta x_1, \Delta x_2)$ are trace intervals in the inline and crossline directions, respectively, restricting the range of the inline wavenumbers $\{-m/2\Delta k_{x,1} \leq k_{x,1} \leq (m/2 - 1)\Delta k_{x,1}\}$ and crossline wavenumbers $\{-n/2\Delta k_{x,2} \leq k_{x,2} \leq (n/2 - 1)\Delta k_{x,2}\}$ is equivalent to low-pass filtering extrapolator $\alpha(\Delta z)$ along spatial directions $\mathbf{x} = (x_1, x_2)$.

A low-pass filter reduces the spatial Nyquist frequency, sample intervals $\Delta \mathbf{x}$ increase correspondingly, and spatial variation of α is, effectively, smoothed. BL operators, therefore, perform well in media with smooth variation in velocity.

When velocity variation is linear (for example, as for a dipping stratigraphic sequence; Figure 4), the BL operator returns good accuracy for low cost compared to PSPI. BL operators suffer, however, where velocity variation is discontinuous, as in a sediment-to-salt transition (Figure 3). Compared to the PSPI approximation, the BL approximation is very poor.

Standard PSPI (Gazdag and Sguazzero, 1984) is improved by applying $e^{i\Delta z[k(\mathbf{x}) - \bar{k}_j]}$ as a correction (equation 15), and a similar approach is used for the BL operator. Because spatial

variation in α corresponds directly to spatial variation in slowness $k(\mathbf{x})$, let $\tilde{k}(\mathbf{x}) = \text{FILT}_{\text{low pass}}\{k(\mathbf{x})\}$ and apply correction $e^{i\Delta z[k(\mathbf{x}) - \tilde{k}(\mathbf{x})]}$ to equation 21 so that

$$\begin{aligned} \psi(\mathbf{x}, z + \Delta z) \\ \approx e^{i\Delta z[k(\mathbf{x}) - \tilde{k}(\mathbf{x})]} \frac{1}{(2\pi)^2} \int_{-\infty}^{\infty} \tilde{\varphi}(\mathbf{k}_x, z + \Delta z) e^{-i\mathbf{k}_x \cdot \mathbf{x}} d\mathbf{k}_x, \end{aligned} \quad (23)$$

where $\tilde{\varphi}$ is given by equation 22. Equation 23 is an efficient approximation to extrapolated wavefield $\psi(z + \Delta z)$.

COST

Any one-way operator can be made to return high accuracy for a large phase angle by setting n in equation 9 to a large value. For the BL operators, we increase the range of wavenumbers in equation 22.

Computational cost (by inspection of equation 10) is proportional to the cost of the FFT scaled by the value chosen for n . Exact cost, of course, is specific to the computational circumstances of the user and is a function of machine architecture, compiler, and the cunning of the resident programmer. For generality of comparison between operators, we restrict our calculations to the number of FFTs required for extrapolation by each. For $n=4$ (a common value for ω - x and GS), for example, cost is $\propto 5 \times MN \log MN$. This includes the FFTs associated with the sum, plus the initial $\text{FFT}_{x \rightarrow k_x}$ of the input wavefield. Then, assuming that the cost of stabilizing ω - x and GS is $\propto 1$ FFT, total cost is $6 \times MN \log MN$, or

$$\text{cost}_{\omega-x, GS} = (n_{\text{terms}} + 2)MN \log MN, \quad (24)$$

where n_{terms} is the number of terms in the ω - x operator (Holberg, 1988) and/or the GS operator (Le Rousseau and de Hoop, 2001).

For PSPI, computational cost is related to the number of reference velocities times the cost of the FFT, plus the cost of the $\text{FFT}_{x \rightarrow k_x}$ of the input wavefield, plus a single FFT for stabilization:

$$\text{cost}_{PSPI} = (n_{\text{ref}} + 2)MN \log MN, \quad (25)$$

where n_{ref} is number of reference velocities. In this comparison, the cost of four-term ω - x and GS ($n_{\text{terms}} = 4$ in equation 24) is equivalent to a PSPI operator with four reference velocities ($n_{\text{ref}} = 4$ in equation 25).

For optimal selection of v_j and Ω_j in the PSPI operator, we modify the method of Bagaini et al. (1995). We force the number of velocity bins to be fixed (in this case, $N_{\text{bins}} = 4$) and then allow the Bagaini et al. (1995) algorithm to determine v_j and Ω_j .

BL operators take advantage of sparse convolution in the wavenumber domain. According to equations 21 and 22, cost is $\propto \text{FFT}_{x \rightarrow k_x}$ of the input, plus $NMnm$ to compute $\tilde{\varphi}$ (equation 22), plus $\text{FFT}_{k_x \rightarrow x}$ of the output (the cost of stabilization is included in this last FFT). The total cost is

$$\text{cost}_{BL} = NMnm + 2MN \log MN. \quad (26)$$

The ranges of n and m in equation 22 for a BL operator equivalent in cost to four-term ω - x and GS operators and a four-reference velocity PSPI operator correspond to $nm = 4 \log MN$.

PHASE ERROR

One-way extrapolators are compared here by analyzing phase error relative to the phase k_z (equation 8) of the Fourier integral operator (equation 6). For ω - x and GS, phase error is computed using

$$\begin{aligned} \Delta k_z(\mathbf{x}, \mathbf{k}_x) &= k_z(\mathbf{x}, \mathbf{k}_x) - \tilde{k}_z(\mathbf{x}, \mathbf{k}_x) \\ &= k(\mathbf{x}) \left[\sqrt{1 - \left(\frac{|\mathbf{k}_x|}{k(\mathbf{x})} \right)^2} - 1 \right] \\ &\quad - \tan^{-1} \left[\frac{\Im\{F_{op}(\mathbf{x}, \mathbf{k}_x)\}}{\Re\{F_{op}(\mathbf{x}, \mathbf{k}_x)\}} \right], \end{aligned} \quad (27)$$

where $\Im\{F_{op}\}$ and $\Re\{F_{op}\}$ represent the real and imaginary parts, respectively, of general operator F_{op} . For the case $F_{op} = F_{\omega-x}$,

$$F_{\omega-x}(\mathbf{x}, \mathbf{k}_x) = \sum_{j=0}^n \gamma_j(\mathbf{x}) |\mathbf{k}_x|^{2j}, \quad (28)$$

and when $F_{op} = F_{GS}$,

$$F_{GS}(\mathbf{x}, \mathbf{k}_x) = e^{i\Delta z[k_z(\mathbf{k}_x) - \tilde{k}]} \left[1 + i\Delta z \sum_{j=1}^n \lambda_j(\mathbf{x}) \kappa_j(\mathbf{k}_x) \right]. \quad (29)$$

Phase error for the PSPI and BL operators can be computed directly using

$$\begin{aligned} \Delta k_z(\mathbf{x}, \mathbf{k}_x) &= k(\mathbf{x}) \left[\sqrt{1 - \left(\frac{|\mathbf{k}_x|}{k(\mathbf{x})} \right)^2} - 1 \right] \\ &\quad - \hat{k}(\mathbf{x}) \left[\sqrt{1 - \left(\frac{|\mathbf{k}_x|}{\hat{k}(\mathbf{x})} \right)^2} - 1 \right], \end{aligned} \quad (30)$$

where $\hat{k} = \omega/v_{PSPI}$ for PSPI, and $\hat{k} = \omega/v_{BL}$ for BL.

If one considers the Li correction (Li, 1991), phase error for the ω - x operator is computed for one reference velocity at a limited number of depths and is applied as a correction by stationary-phase shift (Etgen and Nichols, 1999). Instead of applying an approximate correction for one operator, we estimate the nonstationary (space variable) phase error for all available operators (here ω - x , GS, PSPI, and BL) for each depth, and then select the operator with the smallest error for a fixed computational cost. (Alternatively, for a fixed error, we could select the operator with the lowest cost.)

The cost of estimating phase error must, of course, be negligible relative to the cost of extrapolation. This means we need to reduce the range of analysis using a physical argument.

ERROR IN LATERAL POSITION

From Figure 5, for phase angle ϕ , distance r is the distance traveled by a plane wave in the (x, y) plane after extrapolation through depth interval Δz :

$$r = \Delta z \tan \phi = \Delta z \frac{|\mathbf{k}_x|}{k_z}. \quad (31)$$

To first order, the error (Δr) in the length of r associated with phase error Δk_z is

$$\begin{aligned} \Delta r &= \frac{\partial r}{\partial k_z} \Delta k_z \\ &= -\Delta z \frac{|\mathbf{k}_x|}{k_z^2} \Delta k_z, \end{aligned} \quad (32)$$

so that the fractional error (ϵ_r) in r is given by

$$\epsilon_r = -\frac{\Delta k_z}{k_z}. \quad (33)$$

Because error increases monotonically with \mathbf{k}_x , we need only compute the error function for a user-defined maximum-phase angle ϕ_{MAX} so that

$$k_{x,MAX} = k(\mathbf{x}) \sin \phi_{MAX}. \quad (34)$$

Then, for lateral variation, the rms error ϵ_{rms} is computed to represent the average error for a given depth:

$$\epsilon_{rms} = \sqrt{\frac{1}{N} \sum_{j=1}^N [\epsilon_r(\mathbf{x}_j, k_{x,MAX})]^2}, \quad (35)$$

where N is the number of traces. Computation of ϵ_{rms} for every available operator adds only a small cost to extrapolation, and results in an operator plan for imaging.

An example of an operator plan is given in Figure 6. At each depth level in the velocity model, ϵ_{rms} is computed using equation 35 for a number of operators. Initially set to zero, a matrix of dimension $N_z \times N_{op}$ is constructed, where N_z is the number of depth levels, and N_{op} is the number of available operators. For each depth, the $\text{MIN}(\epsilon_{rms})$ is found, and integer 1 is written to the column of the corresponding operator. The matrix represents the operator plan and is included as input to imaging. Then, for each $j * \Delta z$ during imaging, where $1 \leq j \leq N_z$, where N_z is the total number of depths to image, use the operator that corresponds to true being returned

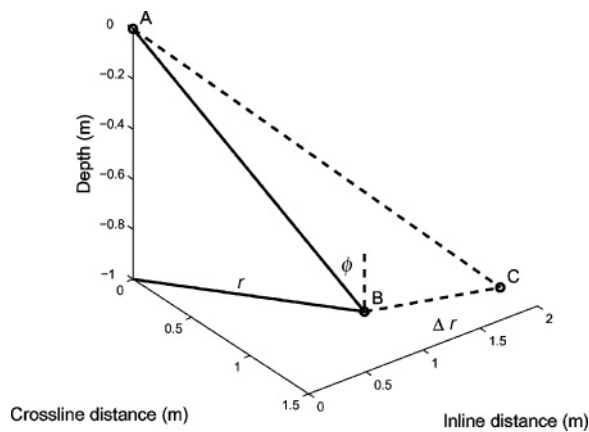


Figure 5. Comparison of exact and approximate phase shift. Segment AB is a ray originating at point A and propagating through depth Δz , and r is the lateral distance traveled. Segment AB represents one-way propagation of a wavefront by exact phase shift. Segment AC is the ray corresponding to an approximate phase shift. Positioning error Δr is shown as a function of inline error Δx and crossline error Δy .

from the following if statement: if $\text{OP_MAT}(j, k) = 1$, where OP_MAT is the $N_z \times N_{op}$ operator matrix, and $1 \leq k \leq N_{op}$.

EXAMPLE

The SEG/EAGE salt model (Aminzadeh et al., 1996) shown in Figure 6 (right side) represents a salt body embedded in smoothly varying sediments in the Gulf of Mexico. Zero-offset data (Figure 7) are derived for this study using 2D finite differences. The data are used as the basis for an imaging comparison between a set of standard imaging algorithms and the plan-based algorithm (Figure 8); the velocity model

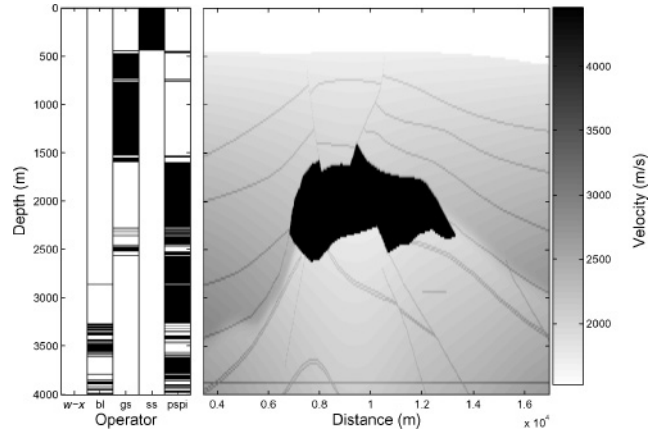


Figure 6. Operator plan for a 2D section of the EAGE/SEG salt model for $\omega = 30$ Hz, $\phi_{MAX} = 70^\circ$, and a fixed cost $\propto 6 \times \text{FFT}_{N=1024}$. Columns on the left represent the five operators used in this study: $65^\circ \omega$ -x, band limited (BL), generalized screen (GS), split step (SS), and phase shift plus interpolation (PSPI). For each level, the most accurate operator is indicated by black fill in the corresponding column. On the right is the velocity profile (not to scale).

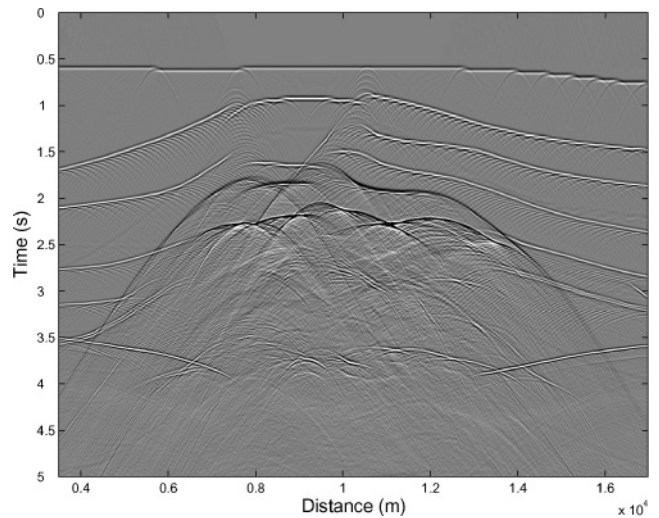


Figure 7. Zero offset data. Finite differences are used to derive these data based on the EAGE/SEG salt model in Figure 6. The depth interval used in modeling is 4 m, and the trace interval is 20 m. The sample interval is 0.002 s. The number of traces displayed is 675. For imaging, the data are padded to 1024 traces, and a record length of 6 s is used.

is unsmoothed except for an antialias filter applied during resampling of the depth axis from 20-m to 4-m intervals.

A number of migration algorithms are used to image the data, and these are summarized in Table 3. Each is parameterized so that for each ω and Δz , computational cost $\propto 6 \times \text{FFT}_{N=1024}$, where $N=1024$ is the number of traces including the zero pad. For the ω - x , GS, and PSPI operators, parameterization means that n in equation 10 is set to 4 (equations 24 and 25). For BL, equation 22 is parameterized with $n=4 \log 1024=28$ (equation 26, $m=1$), and the sum over m is ignored. Of course, cost varies with implementation; we use this group of operators merely as a demonstration.

Generally, the ω - x -based algorithm provides a good image (Figure 9a), and the base reflector is properly imaged as flat. Exceptions are in the steepest parts of the salt body between depths 1500 and 2500 m at 7000 m distance, and between depths 1500 and 1700 m at 10 000 m distance. For stability, the $65^\circ\omega$ - x algorithm is implemented with a high-cut filter for angles $>65^\circ$, so steeper dips are filtered. The GS algorithm images the steep dips in the upper part of the salt (Figure 9b), but the base reflector is not flattened.

An image derived using a split-step Fourier (SS) algorithm is presented in Figure 10a as a check on the GS algorithm. GS

provides a superior image to SS everywhere in the model, and confirms the superiority of this relatively new operator.

The velocity contrast between the sediments and the salt top is too strong for the BL operator (Figure 10b), and any attempt at stabilization (for example, forcing a 65° cutoff) fails, and the algorithm “blows up” near the top of the salt. Of course, instability is intrinsic to explicit, one-way operators (Etgen, 1994), and amplitudes can grow with recursion, as is demonstrated catastrophically here. Fortunately for the plan-based method, as will be seen, stability is seen in the levels in the model that are extrapolated optimally with BL.

The image using a PSPI algorithm and four reference velocities is given in Figure 11a. It is equivalent in quality to the ω - x image (Figure 9a) except for the steepest parts of the salt, where PSPI is superior. PSPI also returns better focusing below the salt when compared to GS (Figure 9b).

Table 3. Imaging algorithms.

Algorithm	Implementation
ω - x	65°
GS	4 term
BL	28 diagonals
PSPI	4 reference velocities

For this work, each algorithm has a computational cost $\propto 6 \times \text{FFT}$ per depth step per temporal frequency.

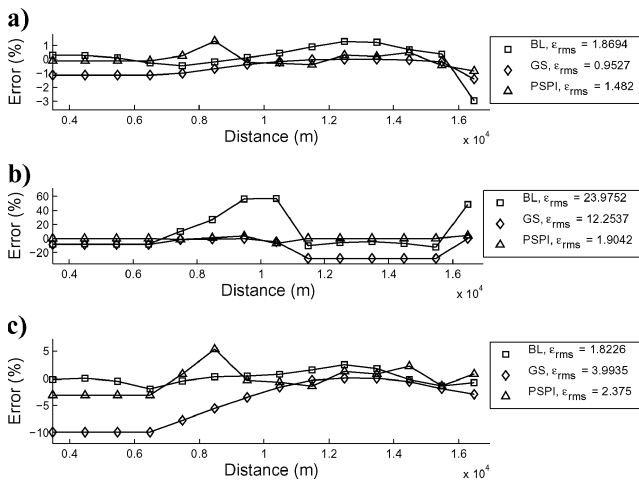


Figure 8. Lateral positioning error for three depths. The rms error ϵ_{rms} for each operator is recorded in the legend. (a) $z=1000$ m. Above the salt, the best operator is the generalized screen (GS) operator. The band-limited operator (BL) is the least accurate. (b) $z=2000$ m. Within the salt, phase shift plus interpolation (PSPI) is most accurate, and BL is the least accurate. (c) Below the salt, a zone centered on $z=3500$ m favors BL, with GS the least accurate.

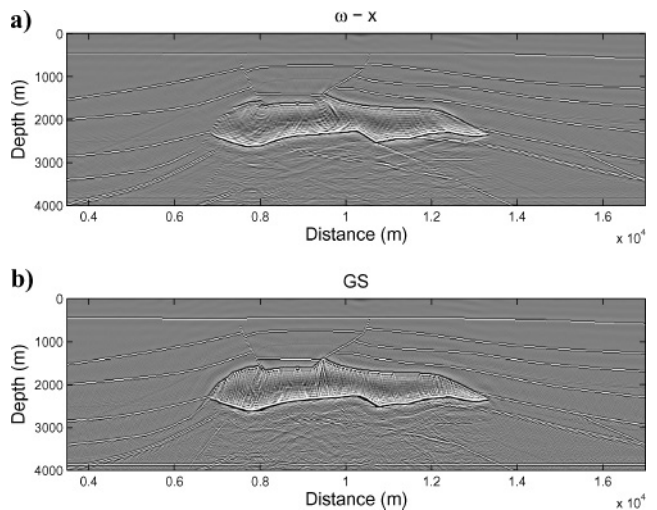


Figure 9. Zero-offset migration of the EAGE SEG salt model. (a) $65^\circ\omega$ - x . (b) Generalized screen (GS).

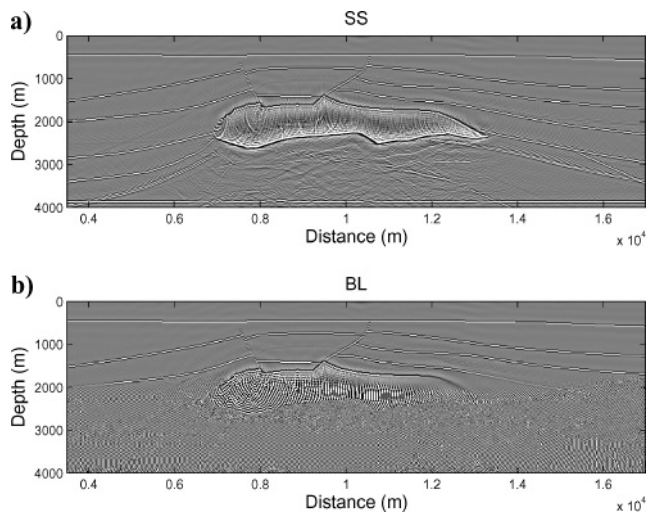


Figure 10. Zero-offset migration of the EAGE SEG salt model. (a) Split-step Fourier (SS). (b) Band-limited (BL). Here, lateral variation through the salt causes instability in the BL operator.

Though the PSPI image looks very good, an improved image is still possible according to the operator plan of Figure 6 (black fill in a column indicates optimal extrapolation for that depth using the corresponding operator). The operator plan is based on the analysis of lateral positioning error ϵ_{rms} (equation 35) for $\omega = 30$ Hz and $\phi = 70^\circ$. The operator with the minimum ϵ_{rms} for each level is selected as the operator for the corresponding depth interval.

In the water column, the SS operator is selected because, along with GS, PSPI, and BL, it is exact in constant velocity but is cheaper than the others by about half. Because the ω - x limits the data to $\phi \approx 65^\circ$, this operator is not considered in the operator plan.

In the sediments above the salt, we find that GS is the most accurate of the available operators. This is demonstrated for $z = 1000$ m in Figure 8a. Here, the minimum lateral positioning error of $\epsilon_{rms} \approx 1\%$ corresponds to the GS operator, while PSPI ($\epsilon_{rms} \approx 1.5\%$), and BL ($\epsilon_{rms} \approx 2\%$) return slightly larger errors.

In the body of the salt, (for example at $z = 2000$ m in Figure 8b), the BL operator returns a very large error ($\epsilon_{rms} = 24\%$), and GS is twice as accurate as the BL operator ($\epsilon_{rms} \approx 12\%$), with PSPI the most accurate, having $\epsilon_{rms} \approx 2\%$. Through most of the salt, therefore, PSPI should be used.

Beneath the salt, PSPI is the favored operator with the exception of a small range of depths around 3500 m. Through this zone (for example, at $z = 3500$ m in Figure 8c), the BL operator is the most accurate with $\epsilon_{rms} \approx 2\%$, followed by PSPI ($\epsilon_{rms} \approx 2.5\%$) and GS ($\epsilon_{rms} \approx 4\%$).

These findings are consistent with the discussion of the individual operators in the "Selection of operators" section. GS performs well in the moderate lateral contrast of the upper sediments, and PSPI performs well at depths corresponding to the sediment/salt interface. BL tends to perform poorly, with the exception of zones below the salt that correspond to linear contrast in velocity.

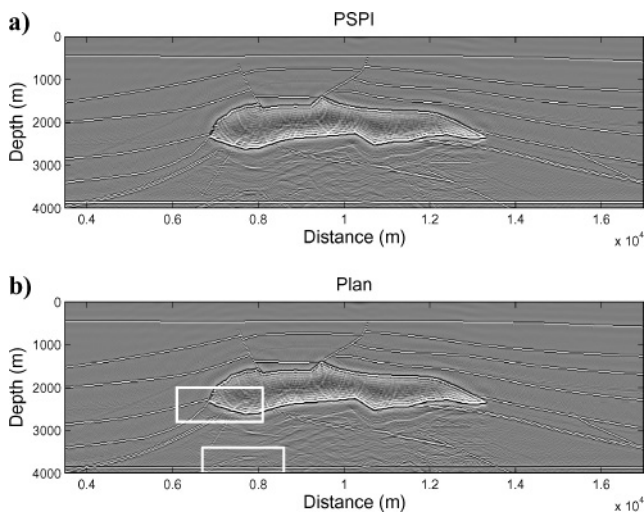


Figure 11. Zero-offset migration of the EAGE/SEG salt model. (a) Phase shift plus interpolation (PSPI). (b) Plan based. The white boxes correspond to the zoom regions of Figures 12 and 13.

The image resulting from a plan-based migration is given in Figure 11b. For the plan-based algorithm, the SS, GS, BL, and PSPI operators are collected, and an if statement is used to assign the optimal operator to a given layer based on the operator plan. Improvements in the image over the PSPI image, for example, are not obvious until we zoom in on specific features, as in Figures 12 and 13.

Truncation of a sediment/sediment reflection against the salt is shown in Figure 12. The plan-based algorithm returns the best image of this structure (Figure 12f) with superior focusing compared to the next-best image of PSPI (Figure 12c), and better imaging of the steep dips compared to ω - x , SS, and GS (Figure 12a, 12b, and 12d, respectively).

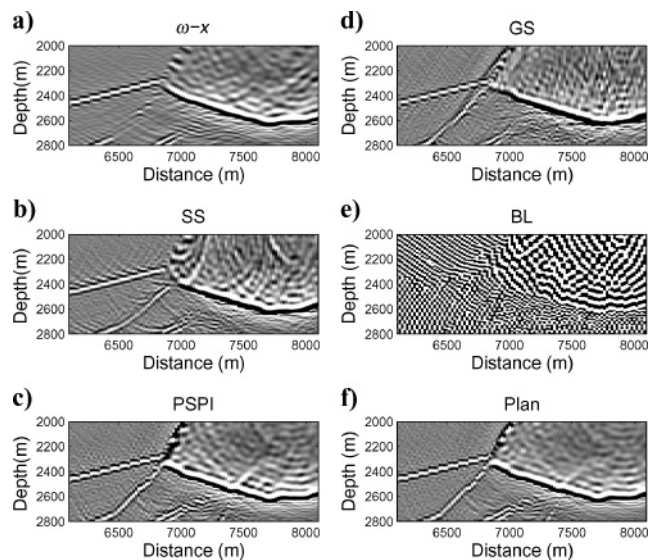


Figure 12. Scale image of a sediment/sediment reflection truncated against the salt. (a) $65^\circ\omega$ - x . (b) Split-step Fourier (SS). (c) Phase shift plus interpolation (PSPI). (d) Generalized screen (GS). (e) Band limited (BL). (f) Plan based.

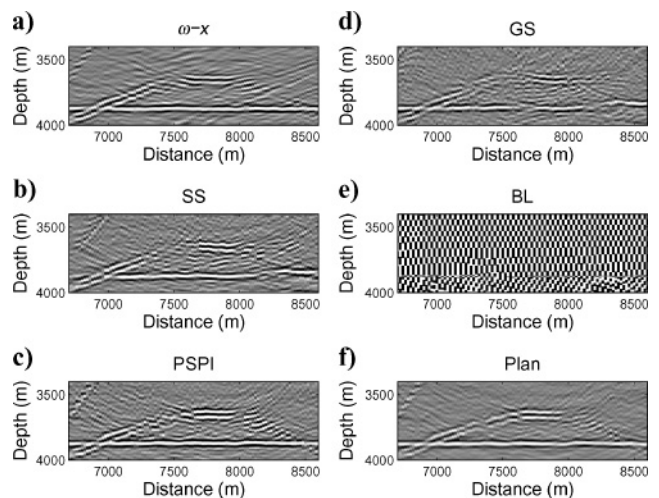


Figure 13. Scale image of a subsalt anticline. (a) $65^\circ\omega$ - x . (b) Split-step Fourier (SS). (c) Phase shift plus interpolation (PSPI). (d) Generalized screen (GS). (e) Band limited (BL). (f) Plan based.

The image of a subsalt anticline is shown in Figure 13. Again, the plan-based algorithm returns the best image (Figure 13f), with enhanced focusing of the left limb of the anticline relative to the other methods.

CONCLUSIONS

We use a general description of one-way extrapolation to relate the cost and accuracy of one-way extrapolation operators. We demonstrate that, because computational cost is proportional to the cost of the fast Fourier transform for most operators and because imaging error is related to phase error, cost and accuracy have a simple relationship. To provide a physically meaningful basis for analysis, we relate phase error to error in lateral position. This results in an efficient framework from which selection of operators for imaging can be tailored to each depth interval in a model. Because each operator is implemented such that cost per depth interval is $\propto 6 \times \text{FFT}_{N=1024}$, an improved image is provided for no additional cost.

ACKNOWLEDGMENTS

We thank the Geology Foundation and the sponsors of the Exploration Development Geophysics Education and Research (EDGER) Forum, University of Texas, Austin, as well as the sponsors of the Consortium for Research in Elastic Wave Exploration Seismology (CREWES), University of Calgary, for supporting this work.

APPENDIX A

THE DISCRETE NONSTATIONARY FILTER IN THE FOURIER DOMAIN

To derive equation 18, it is sufficient to consider one spatial dimension in either the inline or crossline direction. Discrete convolution of nonstationary filter $\tilde{A}(\Delta z)$ and spectrum $\varphi(z)$ is

$$\varphi_j(z + \Delta z) = \sum_{k=-M/2}^{M/2-1} \varphi_k(z) \tilde{A}_{j-k,k}(\Delta z), \quad (\text{A-1})$$

where M is the number of traces. \tilde{A} is a band-limited version of spectrum A :

$$\tilde{A}_{q,k} = \sum_{p=-m/2}^{m/2-1} A_{p,k} \delta_{p,q}, \quad (\text{A-2})$$

where $m \leq M$ and

$$A = FT_x\{\alpha\} \quad (\text{A-3})$$

is extrapolator α Fourier transformed along spatial coordinate x . Substitution of equation A-2 into equation A-1 gives

$$\varphi_j(z + \Delta z) = \sum_{k=-M/2}^{M/2-1} \varphi_k(z) \sum_{p=-m/2}^{m/2-1} A_{p,k}(\Delta z) \delta_{p,j-k}, \quad (\text{A-4})$$

and summing over index k gives

$$\varphi_j(z + \Delta z) = \sum_{p=-m/2}^{m/2-1} \varphi_{j-p}(z) A_{p,j-p}(\Delta z). \quad (\text{A-5})$$

REFERENCES

- Aminzadeh, F., N. Burkhard, J. Long, T. Kunz, and P. Duclos, 1996, Three dimensional SEG/EAEG models — An update: *The Leading Edge*, **15**, 131–134.
- Bagaini, C., E. Bonomi, and E. Pieroni, 1995, Data parallel implementation of 3-D PSPI: 65th Annual International Meeting, SEG, Expanded Abstracts, 188–191.
- Benson, A. K., 1995, Phase-shift migration with a variable-length spatial transform — An algorithm for moderately varying lateral velocities: *Geophysical Prospecting*, **43**, 729–741.
- Berkhout, A. J., 1979, Steep dip finite-difference migration: *Geophysical Prospecting*, **27**, 196–213.
- , 1985, *Seismic migration: Imaging of acoustic energy by wavefield extrapolation*: Elsevier.
- Black, J. L., C. B. Su, and C. B. Wason, 1984, Steep-dip depth migration: 54th Annual International Meeting, SEG, Expanded Abstracts, 456–457.
- Claerbout, J. F., 1971, Toward a unified theory of reflector mapping: *Geophysics*, **36**, 467–481.
- Duistermaat, J. J., 1995, *Fourier integral operators*: Springer-Verlag.
- Etgen, J. T. E., 1994, Stability of explicit depth extrapolation through laterally varying media: 64th Annual International Meeting, SEG, Expanded Abstracts, 1266–1269.
- Etgen, J., and D. Nichols, 1999, Application of the Li correction to explicit depth-extrapolation methods: 69th Annual International Meeting, SEG, Expanded Abstracts, 1366–1369.
- Fishman, L., and J. J. McCoy, 1985, A new class of propagation models based on a factorization of the Helmholtz equation: *Geophysical Journal of the Royal Astronomical Society*, **80**, 439–461.
- Gazdag, J., 1978, Wave equation migration with the phase-shift method: *Geophysics*, **43**, 1342–1351.
- Gazdag, J., and P. Sguazzero, 1984, Migration of seismic data by phase-shift plus interpolation: *Geophysics*, **49**, 124–131.
- Hale, D., 1991, Stable explicit depth extrapolation of seismic wavefields: *Geophysics*, **56**, 1770–1777.
- Han, B., 1998, A comparison of four depth-migration methods: 68th Annual International Meeting, SEG, Expanded Abstracts, 1104–1107.
- Holberg, O., 1988, Towards optimum one-way wave propagation: *Geophysical Prospecting*, **36**, 99–114.
- Hörmander, L., 1965, Pseudo-differential operators: *Communications in Pure and Applied Mathematics*, **18**, 501–517.
- Kessinger, W., 1992, Extended split-step Fourier migration: 62nd Annual International Meeting, SEG, Expanded Abstracts, 917–920.
- Kosloff, D., and D. Kessler, 1987, Accurate depth migration by a generalized phase-shift method: *Geophysics*, **52**, 1074–1084.
- Kumano-Gō, H., 1981, *Pseudo-differential operators*: MIT Press.
- Le Rousseau, J. H., and M. V. de Hoop, 2001, Modeling and imaging with the scalar generalized-screen algorithms in isotropic media: *Geophysics*, **66**, 1551–1568.
- Li, Z., 1991, Compensating finite-difference errors in 3-D migration and modeling: *Geophysics*, **56**, 1650–1660.
- Margrave, G. F., and R. J. Ferguson, 1997, Wavefield extrapolation by nonstationary phase shift: 67th Annual International Meeting, SEG, Expanded Abstracts, 1599–1602.
- , 2000, Taylor series derivation of nonstationary wavefield extrapolators: 70th Annual International Meeting, SEG, Expanded Abstracts, 834–837.
- Nautiyal, A., S. H. Gray, N. D. Whitmore, and J. D. Garing, 1993, Stability versus accuracy for an explicit wavefield extrapolation operator: *Geophysics*, **58**, 277–283.
- Pai, D. M., 1988, Generalized f - k (frequency-wavenumber) migration in arbitrarily varying media: *Geophysics*, **53**, 1547–1555.
- Ristow, D., and T. Ruhl, 1994, Fourier finite-difference migration: *Geophysics*, **59**, 1882–1893.
- Saint Raymond, X., 1991, *Elementary introduction to the theory of pseudodifferential operators*: CRC Press.
- Stoffa, P. L., J. T. Fokkema, R. M. de Luna Freire, and W. P. Kessinger, 1990, Split-step Fourier migration: *Geophysics*, **55**, 410–421.
- Thorbecke, J. W., and A. J. Berkhout, 1994, 3-D recursive extrapolation operators: An overview: 64th Annual International Meeting, SEG, Expanded Abstracts, 1262–1265.
- Wu, R. S., and M. V. de Hoop, 1996, Accuracy analysis of screen propagators for wave extrapolation using a thin-slab model: 66th Annual International Meeting, SEG, Expanded Abstracts, 419–422.
- Wu, R. S., and L. Y. Huang, 1992, Scattered field calculation in heterogeneous media using phase-screen propagation: 62nd Annual International Meeting, SEG, Expanded Abstracts, 1289–1292.
- Wu, R.-S., F. Yang, Z. Wang, and L. Zhang, 1997, Migration operator compression by wavelet transform: Beamlet migrator: 67th Annual International Meeting, SEG, Expanded Abstracts, 1646–1649.